Vol.9, Issue No 3, Sep 2019

# AEOLIAN TONE AND ACOUSTICAL INSULATING PLATE AERODYNAMIC NOISE ASSESSMENT USING SIMILARITY LAW

A.Girish,Sharanappa Koni,S Naveen

Asst. Prof,Asst. Prof,Asst. Prof

girish.hospet@gmail.com, sharanukoni@gmail.com, naveen.rymec40@gmail.com

Department of Mech, Proudhadevaraya Institute of Technology, Abheraj Baldota Rd, Indiranagar, Hosapete, Karnataka-583225

**Abstract**

This study aims to evaluate aerodynamic noise sources and the similarity law's conversion to wind speed as the wind speed increases. The aerodynamic noise emitted by periodically holed and non-holed cylinders, as well as a pantograph model with and without a sound insulating plate, was measured in a low-noise high-speed wind tunnel. As a dipole sound source, the cylinders generated an audible level of noise that increased with the sixth power of the wind speed. Additionally, the noise-reduction effects of the periodic holes—a shift in the flow structure—persisted. The second peak noise coming from the cylinder, however, was proportional to the sum of the sixth and eighth powers of the wind speed, and the wind speed conversion using a dipole sound source was too low. When compared to the pantograph model without the sound insulating plate, the noise level with the plate was proportionally lower than the sixth power of the wind velocity. This is because there was a frequency signature to the sound insulating plate's noise reduction effect. In this study, the dominating pantograph noise frequency area moved to a higher level as the wind velocity increased, and the dominant noise level started to be impacted by the sound insulating plate's noise reduction. Because of the noise level conversion of wind velocity, the sound insulating plate's reduction impact was 2.5 dB understated. Subtracting the pantograph's estimated noise level from the theoretical lowered noise level of the plate, which was determined using the Fresnel number, allowed us to address this issue. The result was pantograph noise, with an estimated sound insulating plate differential of just 0.8 dB.

***Keywords***: Aerodynamic noise, Wind tunnel, High-speed train, Similarity law, Pantograph, Cylinder

## 1. Introduction

The trend of inter-city trains around the world is for them to become faster. To not disturb the environment along railway lines, it is necessary to reduce aerodynamic noise, which increases as a train's running speed increases. To reduce aerodynamic noise, detailed knowledge on the noise distribution and properties of sound sources is necessary. Measuring the noise of full-scale running trains is useful for finding a noise distribution. Martens et al. (2009) identified different noise sources of the German ICE 3 train by using a microphone spiral array, and Kurita (2011) carried out noise measurements on a series E2-1000 train that was running in order to understand which areas generated sound and the contribution to overall noise. However, measuring the noise of full-scale trains requires noise reduction methods, and the cost and time of developing such methods are enormous. Therefore, generally, wind tunnel tests are conducted to evaluate such methods. We measure the radiated aerodynamic noise of a reduced scale model in a wind tunnel and estimate the full-scale noise from the test result by using the similarity law of aerodynamic noise. For example, Yamazaki et al. (2007) investigated noise reduction techniques for the gap section in a 1/8 scale train model in a wind tunnel.

The similarity law is important for accurately estimating full-scale noise from the results obtained with a reduced scale model. The law needs to convert the noise spectrum of a reduced scale model in a wind tunnel into that of a full-scale one by taking the difference between the wind velocity, the scale, and the measurement conditions of the two models into consideration. Iida et al. (2000, 2007) suggested using the law for aerodynamic sound generation to estimate full-scale model noise under conditions that satisfy the flow similarity. In the similarity law, the sound pressure level $SPL$ is in proportion to the sixth power of wind velocity and to the double power of the scale from the sound pressure of a reduced-scale model $SPL_m$. The full-scale frequency $f_r$ [Hz] is acquired from the frequency of a scale model $f_m$ [Hz], wind velocity $U$ [m/s], and characteristic length $D$ [m].

$$SPL_r = SPL_m + 10\log\left(\frac{a_m^2 \rho_r^2}{a^2 \tau^2}\right) + 60\log\left(\frac{U_r}{U}\right) + 20\log\left(\frac{D_r}{D}\right) - 20\log\left(\frac{r_r}{r}\right) \quad (1)$$

$$f_r = \frac{\mathrm{St}}{D}$$

$$= f_m \left( \frac{D_m}{D_r}, \frac{U_r}{U_m} \right) \quad (2)$$

Where $a$ [m/s]: sound speed, ρ [kg/m$^3$]: air density, $r$ [m]: measurement distance. The suffix $m$ means the value of a reduced-scale model, and the suffix $r$ means the value of a full-scale model.

This similarity law is derived from Lighthill-Curle's equation (Lighthill, 1952, Curle, 1955). The equation indicates that the main source of aerodynamic noise is changed from a dipole sound source generated by aerodynamic force fluctuation to a quadrupole sound source generated by flow disturbances, depending on the Mach number. The difference in noise source leads to the similarity law being changed, such as the correlation between wind velocity and aerodynamic noise level. A dipole sound source increases in proportion to the sixth power of wind velocity, and a quadrupole sound source increases in proportion to the eighth power of wind velocity. In Curle's equation, the order of the sound powers $\Pi_d$ and $\Pi_q$, which are directly radiated from a dipole sound source and a quadrupole sound source in a certain volume $V_0$ with a compact body, are approximated as Eqs. (3) and (4) (Kambe, 1988, Howe, 2003). These are calculated from the product of the sound power, which of a dipole sound source and a quadrupole sound source are estimated as $P_D \sim l^2\rho_0 U^6/a^3$ and $P_Q \sim l^2\rho_0 U^8/a^5$, and the number of sources, which are counted as $N_D = A/l^2$ and $N_Q = V_0/l^3$. The ratio of the sound powers $\Pi_q / \Pi_d$ is approximately estimated on the basis of the Mach number as Eq. (5).

$$\Pi_d \sim \frac{l^2\rho_0 U^6}{a^3} \times \frac{A}{l^2} = A\rho_0 U^3 M^3 \quad (3)$$

$$\Pi_q \sim \frac{l^2\rho_0 U^8}{a^5} \times \left(\frac{V_0}{l^3}\right) = \left(\frac{V_0}{l}\right) \rho_0 U^3 M^5 \quad (4)$$

$$\Pi_q / \Pi_d \sim \frac{(V_0)}{A} M^2 \quad (5)$$

Where $A$ [m$^2$]: area of compact body facing turbulent flow, $(= U/a)$ [-]: Mach number, $V_0$ [m$^3$]: a certain volume, $l$ [m]: a turbulent correlation length.

Until now, since the Mach number of the flow around trains has been comparatively small, the aerodynamic noise radiating from trains was regarded as a dipole sound source generated from surface pressure fluctuations. Therefore, we estimate the noise level of full-scale trains in proportion to the sixth power of the train running speed as Eq. (1). However, next generation high-speed trains are expected to run faster, which will probably lead to full-scale estimated noise errors because of the quadrupole sound source of the aerodynamic noise from trains or the difference in wind velocity between reduced-scale and full-scale models.

In this study, to evaluate the change in the similarity law as the wind velocity increases, we measured the aerodynamic noise that radiates from cylinders with and without periodic holes and a reduced-scale pantograph model with and without a sound insulating plate, which is generally used to reduce noise for high-speed trains, when the flow was faster than 100 m/s in a low-noise high-speed wind tunnel. We investigated the correlation between wind velocity and aerodynamic noise level for the cylinder or the pantograph with acoustical insulation and assessed aerodynamic noise sources and wind velocity conversion with the similarity law.

## 2. Experimental Setup

Experiments were performed in a low noise high-speed wind tunnel (Hitachi, 2014, Matsui, 2017). The wind tunnel test section was 600 mm ($W$) × 400 mm ($H$) × 2,000 mm ($L$), and the max flow speed was 116.7 m/s. Figure 1 shows the configuration of the experimental setup. Test models were installed at a location 400 mm from a nozzle, and a microphone (DC53A, Rion) was set up span-wise $D_m$ = 1,000 mm from the center of the models at the same height as a ground plate to reduce the effect of noise reflection. The noise was measured by a sound-level meter (NL-14, Rion) and recorded by a data logger (DS-2000, Ono Sokki). The sampling frequency was 40,000 Hz. The measured data was FFT-analyzed. The number of sampling points was 16,384, and the average number of times was 64.

Two types of test models, two cylinders and a pantograph model, were used. Figure 2 shows the cylinders used in this study. The cylinders, of which the diameter was $d_c$ = 25 mm and the height was $h_c$ = 550 mm, were measured. One of them had 11 periodic holes, of which the width was $w_h$ = 5 mm and length was $l_h$ = 20 mm. It is known that periodic holes reduce aerodynamic noise, especially peak noise, called "Aeolian tone," by preventing Karman vortex shedding (Takaishi et al., 2003).

We also measured the noise that radiated from a 1/10 reduced-scale pantograph model. Generally, to prevent pantograph noise from radiating, sound insulating plates are used in shinkansens (bullet trains) in Japan (Wakabayashi et al., 2008). To evaluate the noise reduction effect of sound insulating plates, pantograph noise with and without a plate was measured. A sound insulating plate was set at the microphone side $D_p$ =150 mm from the center. The height of the plate was $h_i$ = 0.53 $D_p$, and its length $l_i$ = 3.3 $D_p$ with 30-degree bottom corners. The height of the pantograph was $h_t$ = 0.9 $D_p$.

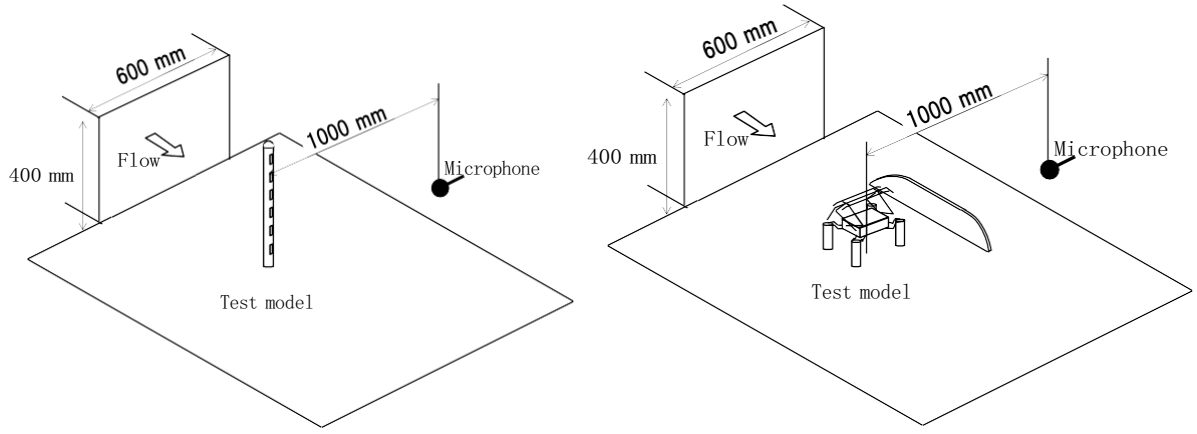


(a) Cylinder (b) Pantograph with sound insulating plate

Fig. 1 Experimental setup

Fig. 2 Cylinders with and without periodic holes

## 3. Experimental Results

### 3.1 Background noise

Figure 3 shows the background noise level of the wind tunnel. The horizontal axis indicates the wind velocity, and the vertical axis indicates the sound pressure level ($SPL$) measured by the sound-level meter. The dashed line is the sum of the sixth and eighth powers, shown as Eq. (6), in which $C$ and $D$ are calculated by using the least square method to minimize the difference from the experimental value. The result shows the contribution of dipole sound and quadrupole

sound in the background noise. In a low-speed region until 60 m/s, the background noise was mainly proportional to the sixth power of wind velocity. This dependence shows that the dominant sound of the background noise was a dipole sound source from the surface pressure fluctuation on the nozzle and collector. In a high-speed region, the background noise became proportional to the eighth power of wind velocity. This dependence shows that the noise generated by the vortex generated from the shear layer at the nozzle became the dominant aerodynamic noise source, that is, a quadrupole sound source.

$$SPL_{est} = 10\log(C \cdot U^6 + \mathrm{D} \cdot U^8) \tag{6}$$

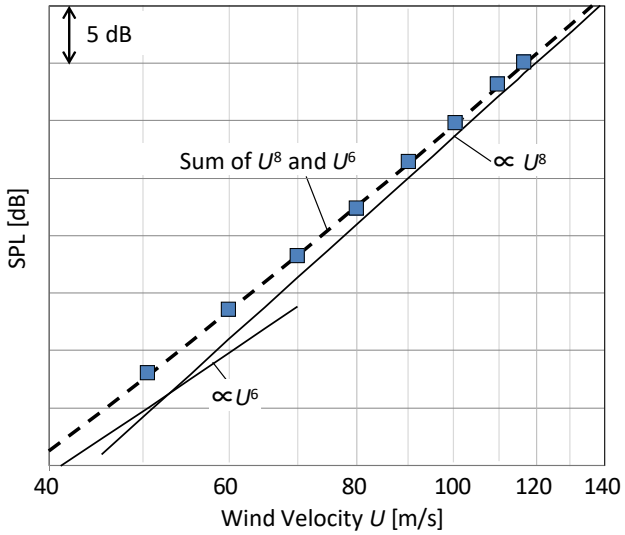


Fig. 3 Background noise level of wind tunnel. Measured value of wind tunnel background noise is plotted with square dots (blue), and dashed line is sum of sixth and eighth powers, which was calculated by least square method to minimize difference from measured value.

### 3.2 Cylinders with and without periodic holes

#### 3.2.1 Cylinder without periodic holes

Figure 4 shows the overall noise level of the cylinders for each wind velocity. The noise level of the cylinder without periodic holes continued to increase in proportion to the sixth power of wind velocity. This indicates that the aerodynamic noise of the cylinder was mainly due to a dipole sound source. It is known that the main noise sources of cylinders is generated from Karman vortices. The Strouhal number, which shows the dimensionless frequency of the Karman vortices from a cylinder, depends on its Reynolds number and changes at a Reynolds number Re of about $1.0 \times 10^6$ due to the laminar-turbulent transition of the boundary layer around a cylinder (Fujita et al., 1999). In this study, the Reynolds number Re based on the cylinder diameter $d_c$ was $1.9 \times 10^5$ at the max wind velocity $U = 116.7$ m/s. It is thought that the Strouhal number $St$ of the Aeolian tone generated by the Karman vortices is constant in this range. Figure 5 shows the frequency analysis results of the measured noise radiating from the two cylinders at 50 and 110 m/s. The dominant peak noise level of the cylinder without periodic holes was found at frequencies $f_{p,1st}$ of 381 Hz (at 50 m/s) and 825 Hz (at 110 m/s). In addition, the second peak noise level was found at peak frequencies $f_{p,2nd}$ of 756 Hz (at $U = 50$ m/s) and 1,633 Hz (at $U = 110$ m/s). Figure 6 shows the Strouhal number $St$ of the peak noise frequencies, the characteristic length of which was set as the cylinder diameter $d_c$. Regardless of wind velocity, the Strouhal number $St$ was constant, the Strouhal number of the first peak was $St_{p,1st} = 0.19$, and that of the second peak was $St_{p,2nd} = 0.38$, which means the vortex formation was constant.

Figure 7 shows the peak noise levels for each wind velocity. The dashed line is the sum of the sixth and eighth powers, shown as Eq. (6), in which $C$ and $D$ are calculated by using the least square method to minimize the difference from the experimental value. The first peak noise level, which was dominant in the noise radiating from the cylinder, increased in proportion to the sixth power of wind velocity. However, the second peak noise level increased in proportion to the sum of the sixth and eighth powers of wind velocity and, the eighth power of wind velocity seems to become dominant over the wind velocity $U = 130$ m/s. This indicates that the second peak noise was changed from a dipole sound source to a

quadrupole sound source. This is because the ratio of noise from the quadrupole source increased at a higher frequency. Generally, representative noise at a higher frequency $f_p$, which is related to wind velocity $U$ and turbulent correlation length $l$ as in Eq. (7), is generated from vortices with a shorter turbulent correlation length $l$. From Eq. (4), a shorter turbulent correlation length $l$ generates a higher noise level from a quadrupole sound source. In this study, it is assumed that the Karman vortices generate sufficient quadrupole sound sources at the second peak noise frequency.

$$f_p \sim \frac{U}{l} \tag{7}$$

This result indicates that the dominant peak noise level of a cylinder increases in proportion to the sixth power of wind velocity as a dipole sound source while vortex formation is steady. However, noise at a higher frequency may increase in proportion to the sum of the sixth and eighth powers of wind velocity because a quadrupole sound source increases due to the shorter turbulent correlation length $l$.

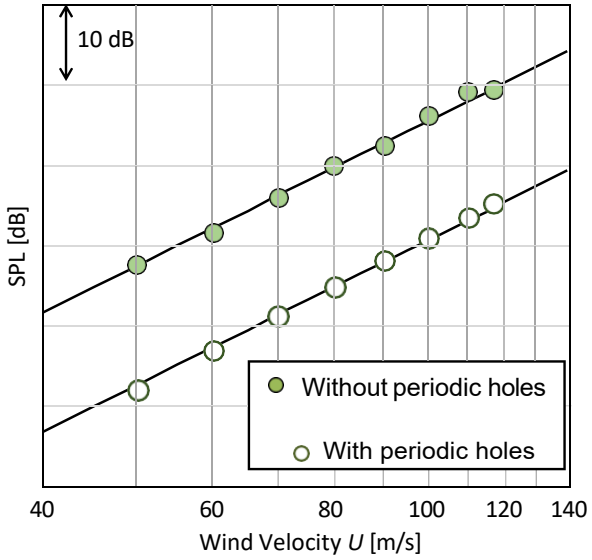


Fig. 4 Overall noise level of cylinders. Measured values of cylinders with and without periodic holes are plotted with white and green dots. Solid line shows sixth power of wind velocity estimated from experimental value.

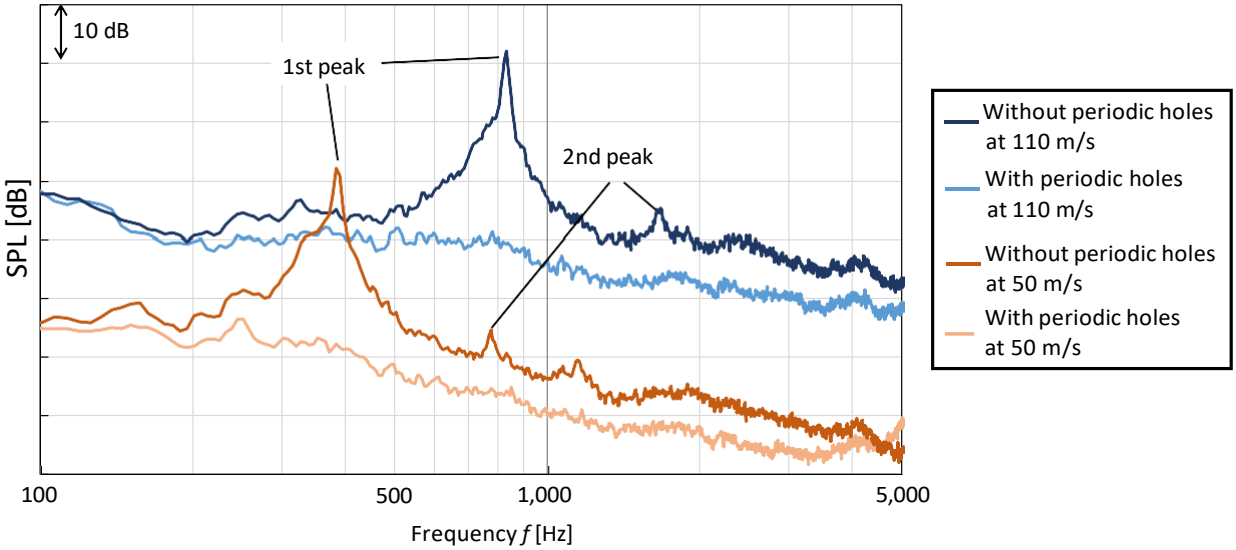


Fig. 5 Comparison of noise level of cylinders at 50 and 110 m/s. Values of cylinders with and without periodic holes measured at 50 m/s are shown with orange and red lines, and those at 110 m/s are shown with blue and black lines.

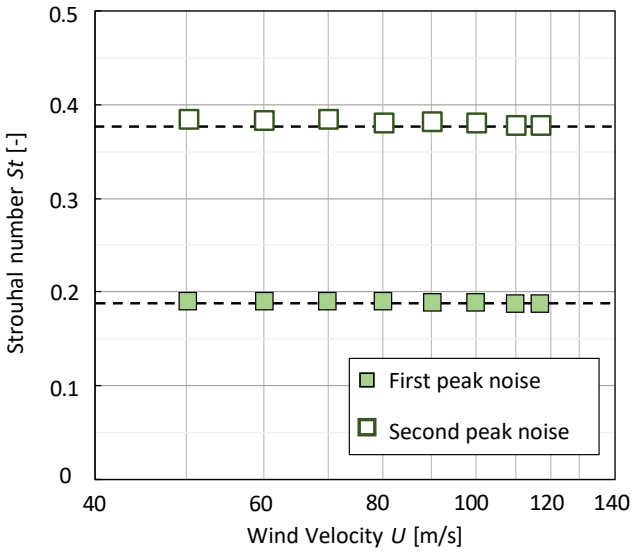


Fig. 6 Strouhal number of first and second peak noise. Measured values of cylinders without periodic holes are plotted with green and white square dots. Dashed line shows average value.

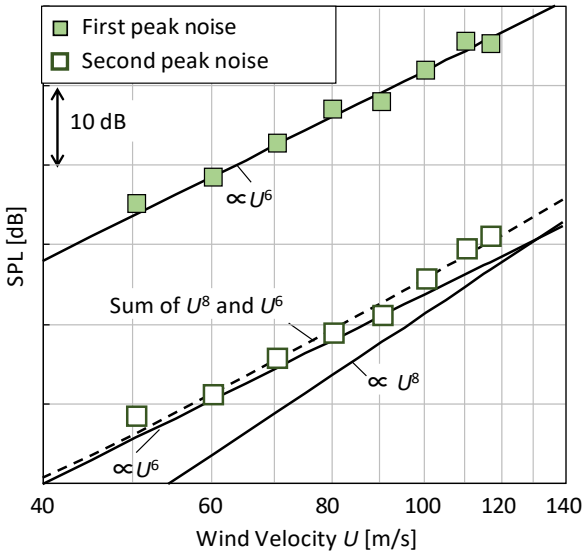


Fig. 7 Peak noise levels of cylinder without periodic holes. Measured values of first and second peak noise are plotted with green and white square dots. Dashed line is sum of sixth and eighth powers of wind velocity estimated from experimental value by least square method.

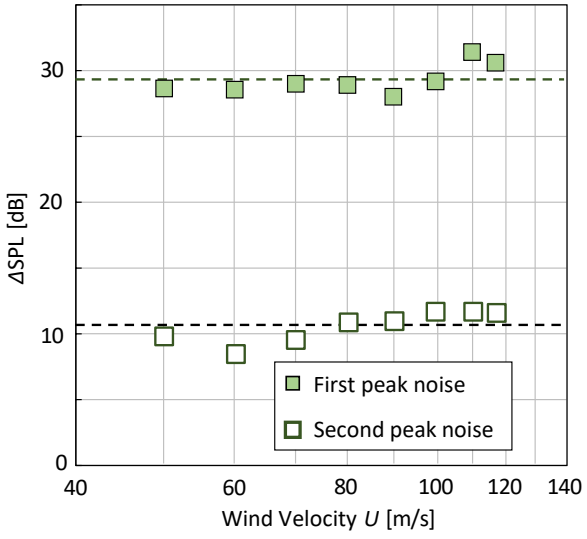


Fig. 8 Reduced noise level of first and second peak noise by periodic holes. Measured values of first and second peak noise are plotted with green and white square dots.

### 3.2.2 Cylinder with periodic holes

Figure 4 also shows the overall noise level of the cylinder with periodic holes. The noise level also increased in proportion to the sixth power of wind velocity. This indicates that the aerodynamic noise of the cylinder with periodic holes was also mainly due to a dipole sound source. In Fig. 5, the periodic holes reduced the noise level, mainly, the peak noise radiated from the cylinder at both 50 and 110 m/s. The periodic holes kept preventing the Karman vortices, which generate peak noise at this Reynolds number. Figure 8 shows the noise level reduced by the periodic holes at the frequency, at which the first and second noise peak was observed. The reduced noise level $\Delta SPL_{p,ed}$ at each wind velocity is estimated by Eq. (8).

$$\Delta SPL_{p,ed} = SPL_{p,without\ \ holes} - SPL_{p,with\ \ holes} \tag{8}$$

Figure 8 indicates that the reduced noise level was almost constant; the reduction of the first and second peak noise was about 29 dB and 11 dB with a difference of 2 dB. In this Reynolds number range, vortex formation was unchanged, and the periodic holes steadily prevented Karman vortex formation and reduced peak noise, regardless of wind velocity.

### 3.2.3 Estimation by similarity law

To evaluate the similarity law, the noise levels of the cylinders with and without periodic holes at a wind velocity of $U$ = 110 m/s were estimated from the measured noise levels at $U$ = 50 m/s in two ways. First, $SPL_{est,d=110m/s}$ was calculated by using Eqs. (2) and (9). Equation (9) is transformed from Eq. (1) for applying only wind velocity conversion. Second, the estimated $SPL_{est,dq}$ was also calculated by using Eqs. (2), (9), and (10). Equation (10) includes the eighth power of wind velocity as a quadrupole sound at more than the second peak noise frequency, $f$ = 1,600 Hz, because the sound level from a quadrupole sound source was almost the same as that from a dipole sound at the second peak noise frequency at a wind velocity $U$ of 110 m/s in Fig. 7.

$$SPL_{est,Vd} = SPL_{mea,=50m/s} + 60\log\left(\frac{110m/s}{50m/s}\right) \tag{9}$$

$$SPL_{est,Vdq} = SPL_{mea,=50m/s} + 0.5\times 60\log\left(\frac{110m/s}{50m/s}\right) + 0.5\times 80\log\left(\frac{110m/s}{50m/s}\right) \quad \text{at } f \geq 1600 \text{ Hz} \tag{10}$$

Figure 9 shows the measured and estimated noise levels of the cylinders with and without periodic holes at wind velocity $U$ = 110 m/s. Figure 9(A) shows that the overall noise levels of the cylinder without periodic holes, $SPL_{est,Vd}$ and $SPL_{est,Vdq}$, were estimated with a 0.9-dB difference from the measured value. This was because the first peak noise, which was the dominant noise for the cylinder without periodic holes, was estimated precisely by using the wind velocity conversion as the sixth power of the wind velocity as a dipole sound source. However, in Fig. 9(A), at more than 1,600 Hz, the estimated $SPL_{est,d}$ was about 4 dB lower than the measured value. This was caused by not including the wind velocity conversion of a quadrupole sound source in $SPL_{est,d}$. In comparison, the estimated $SPL_{est,dq}$ was within 2 dB from the measured value at more than 1,600 Hz. This shows it is important to include the eighth power of wind velocity as a quadrupole sound source in the wind velocity conversion not only just at the second peak but also at higher frequency than the second peak. Fig. 9(b) shows that the overall noise levels of the cylinder with periodic holes were estimated with a 0.5 dB-difference from the measured value. At more than 1,600 Hz, the estimated $SPL_{est,dq}$ was closer to the measured value than $SPL_{est,Vd}$. This result implies the velocity conversion including the eighth power of wind velocity can be adapted to the noise radiated from small vortices, which are not generated from the Karman vortices. These results indicate that the similarity law needs to include the eighth power of wind velocity at a high frequency in order to estimate precisely the noise level, which was more than the second noise peak frequency in this study.

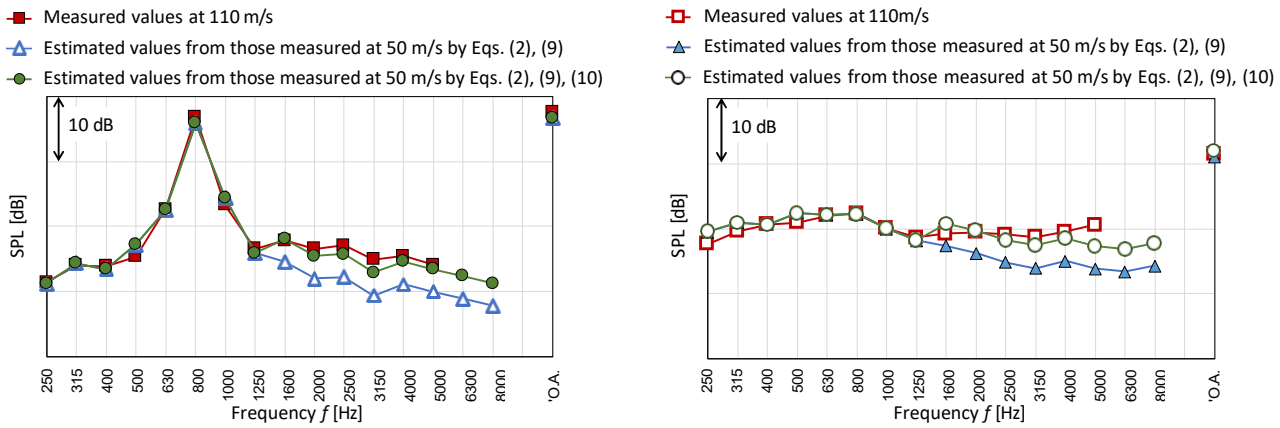


(A) Cylinder without periodic holes (B) Cylinder with periodic holes

Fig. 9 Measured and estimated noise levels of cylinders with and without periodic holes at wind velocity $U = 110$ m/s. Measured values are plotted with square dots. Values estimated by Eqs. (2), (9) and those by Eqs. (2), (9), (10) are plotted with triangle and circle dots.

### 3.3 Pantograph models with and without sound insulating plate

#### 3.3.1 Comparison of pantograph models with and without sound insulating plate

Figure 10 shows the noise level of the full-scale pantograph estimated from the measured values of a 1/10 scale model. The noise level of the pantograph without the sound insulating plate continued to increase in proportion to the sixth power of wind velocity. This indicates that the aerodynamic noise of the pantograph was mainly due to a dipole sound source. It is thought that the dipole sound source generated from surface pressure fluctuations caused by the pantograph's own shape was dominant. However, the noise level of the pantograph model with the sound insulating plate increased in proportion to less than the sixth power of wind velocity. This indicates that the effect of noise reduction with the sound insulating plate increased in accordance with the wind velocity.

Figure 11 shows a comparison of the noise level radiating from the pantograph models with and without the sound insulating plate at 50, 75, and 116.7 m/s. From the comparison of the pantograph without the plate at different wind velocities, it is indicated that the dominant frequency of the pantograph noise increased according to the increase in the wind velocity. This peak frequency was increased from 500 Hz at 50 m/s to 750 Hz at 75 m/s and 1,250 Hz at 116.7 m/s, which shows that its frequency increased in accordance with the Strouhal number, written in Eq. (2). From a comparison of the pantograph with and without the plate at the same wind velocity, it was found that the sound insulating plate reduced the noise level more at a high frequency than at a low frequency. This is because the diffraction of acoustic waves was changed by the noise frequency. Because of its short wavelength, the expansion of high-frequency sound at the edge of the sound insulating plate due to diffraction was prevented, and more noise radiating from the pantograph was cut off. Comparing the pantograph with and without the plate at different wind velocities, it was indicated that the dominant pantograph noise level began to be reduced by the sound insulating plate as the wind velocity increased. The peak noise level of the pantograph model at 116.7 m/s was reduced 2.9 dB by the sound insulating plate in contrast to that at 50 m/s. This resulted from the increase in pantograph peak noise frequency due to the increasing wind velocity and the increase in the sound insulating plate's noise reduction effect at a high frequency. Therefore, the noise reduction effect of the sound insulating plate was increased by increasing the wind velocity. This lead to the pantograph model with the sound insulating plate increasing the noise level in proportion to less than the sixth power of wind velocity.

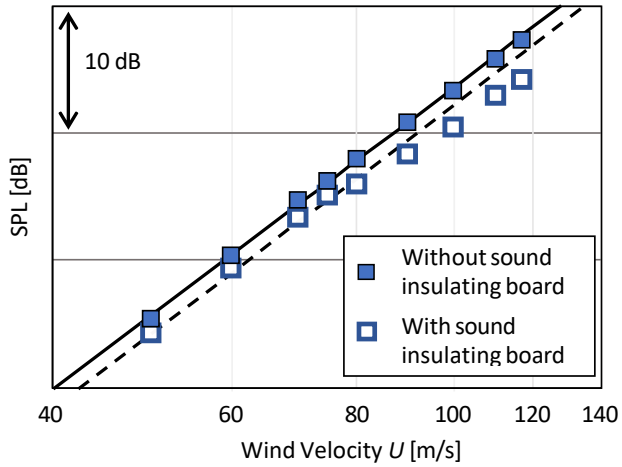


Fig. 10 Overall noise level of full-scale pantograph estimated from measured values of 1/10 scale model. Measured values of pantograph with and without sound insulating board are plotted with white and blue squares. Solid line is sixth power of wind velocity estimated from measured values of pantograph without sound insulating board, and dashed line is that of pantograph with sound insulating board in low-speed region until 80 m/s.

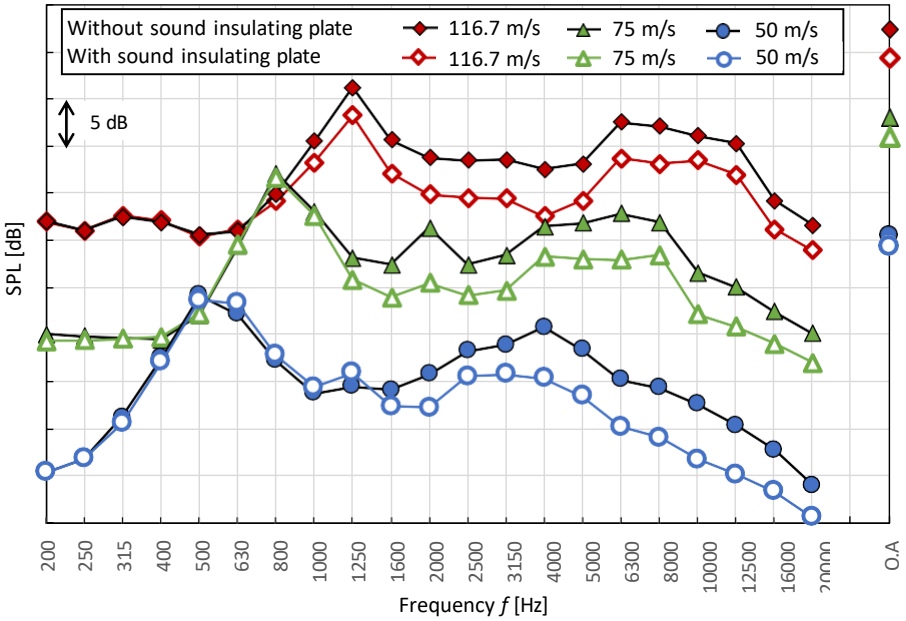


Fig. 11 1/3 octave band frequency analysis of noise from measured values of 1/10-scale pantograph with and without sound insulating plate. Measured values at 116.7 m/s are plotted with red and white rhombus dots. Measured values at 75 m/s are plotted with green and white triangle dots. Measured values at 50 m/s are plotted with blue and white circle dots.

### 3.3.2 Reduction effect of sound insulating plate

To evaluate the reduction effect of the sound insulating plate, the theoretical reduced noise level of the sound insulating plate, $\Delta SPL_{pl,he}$, was estimated from Eqs. (11), (12), and (13).

In Eq. (11), the noise level is reduced by a sound insulating plate with infinite length, $\Delta L$. The Fresnel number $N$ is the ratio of the sound wave length $\lambda$ and the difference in distance $\delta$ among a noise source, the edge of a plate, and a measurement point, of which the position is shown in Fig. 12 (Maekawa 1962, Yamamoto and Takagi 1991). The distance difference $\delta$ was calculated by Eq. (12) and was classified by whether a noise source (NS) can be seen from the measurement point (MP), that means the relation between the height of the plate edge $h_i$ and the height $h_E$ of the line from NS to MP at the plate position in Fig.12. Equation (13) indicated the reduced noise levels of a sound insulating plate with a limited length (Yamamoto et al. 1994). This was calculated from the sum of the noise level through the open areas in the plane of the sound insulating plate. Equation (13) indicates the noise reduction of the square insulating board,

which is shown as the separate areas $C_0$, $C_6$, $C_7$, and $C_8$ in Fig. 13.

$$\Delta L(f) = \begin{cases} 5 + 20\log_{10}\frac{\sqrt{2\pi N}}{\tanh(\sqrt{2\pi N})} & N \geq 0 \\ 5 - 20\log_{10}\frac{\sqrt{-2\pi N}}{\tanh(\sqrt{-2\pi N})} & 0 > N \geq -0.4345 \\ 0 & -0.4345 \geq N \end{cases} \quad (11)$$

Where $N$ [-]: Fresnel number $(= 2\delta/\lambda = 2\delta f/a)$
$\delta$ [m]: difference in distance
$\lambda$ [m]: wavelength of sound $(= a/f)$

$$\delta = \begin{cases} b + c - d & h_E < h_i \\ -(b + c - d) & h_E \geq h_i \end{cases} \quad (12)$$

Where $b$ [m]: distance between noise source and edge of sound insulating plate
$c$ [m]: distance between edge of sound insulating plate and measurement point
$d$ [m]: distance between noise source and measurement point

$$\Delta SPL_{pl,he}(f) = -10\log_{10}\{10^{-\frac{\Delta L_{123}}{10}} + (10^{-\frac{\Delta L_{0-5}}{10}} - 10^{-\frac{\Delta L_{123}}{10}}) \times (10^{-\frac{\Delta L_{146}}{10}} + 10^{-\frac{\Delta L_{358}}{10}})\} \quad (13)$$

Where the suffix shows the number of open areas. For example, $\Delta L_{123}$ means the reduced noise level when areas except $C_1$, $C_2$, $C_3$ are assumed as a sound insulating plate with infinite length.

The theoretical reduction noise level of the sound insulating plate was calculated by Eqs. (11) - (13) for each 1/3 octave band frequency region. In this study, it was supposed that the noise source of the pantograph was set at its body and panhead. The panhead height was $h_t = 0.9\ D_p$ and the body height was $h_b = 0.5\ D_p$. To easily estimate $\Delta L_{146}$ and $\Delta L_{358}$ in Eq. (13), the shape of sound insulating plate was assumed to be square, of which the height was $h_i = 0.53\ D_p$ and the length was $l_p = 0.6\ l_i$ as shown in Fig.13. In this study, the measurement point is at the side from the center of the sound insulating board and at the height of the ground plane, which means $\Delta L_{146} = \Delta L_{358}$ and $\Delta L_{0\text{-}5} = 0$. This leads to Eq. (14) from Eq. (13).

$$\Delta SPL_{pl,he}(f) = -10\log_{10}\{10^{-\frac{\Delta L_{123}}{10}} + (1 - 10^{-\frac{\Delta L_{123}}{10}}) \times 2 \times 10^{-\frac{\Delta L_{146}}{10}}\} \quad (14)$$

Figure 14 shows the theoretical and measured noise levels reduced by the sound insulating plate. From Fig.14, the theoretical levels were different due to the position of the source. At a high frequency region, the theoretical values from the pantograph body increased and, in contrast, those from its panhead decreased. This is because the Fresnel number, $N$, was changed at a high frequency. The sound insulating plate hid the pantograph body and prevented the sound from reaching the measurement point, which leads the reduction in noise effect to increase at a high frequency. However, the panhead of the pantograph can be seen from the measurement point and the sound radiating from the panhead was mainly reduced by the diffraction of the plate. This resulted in a decrease of the noise reduction at a high frequency, at which the sound wavelength was short, according to Eq. (11). And, the reduction of noise from the panhead by sound insulating plate also decreased at a low frequency. This is because the sound insulating plate, at a low frequency, reduced less noise through the side of the sound insulating plate, which means $C_1$, $C_3$, $C_4$ and $C_5$ in Fig. 13. Equation (14) shows that the less reduction of the noise through the side of the plate decreases the total noise reduction of the plate. Therefore, the reduction of noise from the panhead by the plate had a peak around 2,000 Hz.

The measured values were the difference between with and without the sound insulating plate in Eq. (15).

$$\Delta SPL_{pl,es} = SPL_{\ without\ plate} - SPL_{\ with\ plate} \quad (15)$$

In Fig. 14, pantograph noise over about 1,250 Hz was reduced by the sound insulating plate, and the reduction level over 3,150 Hz was in the range between the theoretical values from its body and those from its panhead. The experimental reduction effect of the plate was small at a low frequency. This was thought to be caused by the experimental reduction of noise through the side of the sound insulating plate being lower than the theoretical one. From Eq. (14), the reduction of noise through the side of the sound insulating plate influences the total noise reduction. And, in this study, the plate length, $l_i = 3.3\ D_p$, equaled the twice of sound wavelength at about 1,360 Hz, which may be too short to decrease the

reduction effect at a low frequency range. Comparing different wind velocity results, the noise reduction frequency range expands toward a low frequency, and the noise reduction level at a high frequency decreased as the wind velocity increased. This is because the noise source position of the pantograph was changed by the wind velocity. According to the Strouhal number shown in Eq. (2), the frequency of the main pantograph noise increases, and this sound may come to be affected by the noise reduction of the plate. From the results above, the experimental noise reduction effect was small at a low frequency and approximate to the theoretical values at a high frequency.

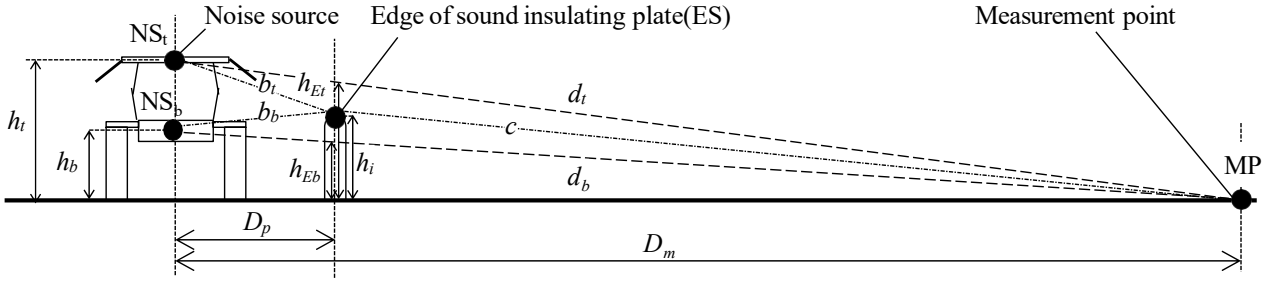


Fig. 12 Positions of noise source, edge of plate, and measurement point. Distances $b_t$ and $b_b$ are between noise source and edge of sound insulating plate. Distance $c$ is between edge of sound insulating plate and measurement point. Distances $d_t$ and $d_b$ are between noise source and measurement point. In this study, noise source of pantograph was supposed to be set at its body $NS_b$ and its panhead $NS_t$.

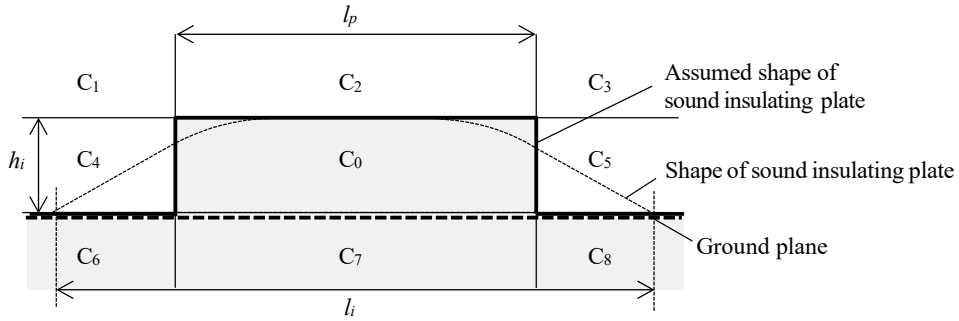


Fig. 13 Areas of sound insulating plate with limited length at plate plane. Equation (12) indicates noise reduction of plate, which is shown as separate areas $C_0$, $C_6$, $C_7$ and $C_8$. Experimental real plate is shown as dashed line. In this study, plate shape was assumed to be square area $C_0$, shown by bold solid line, to easily calculate noise reduction effect.

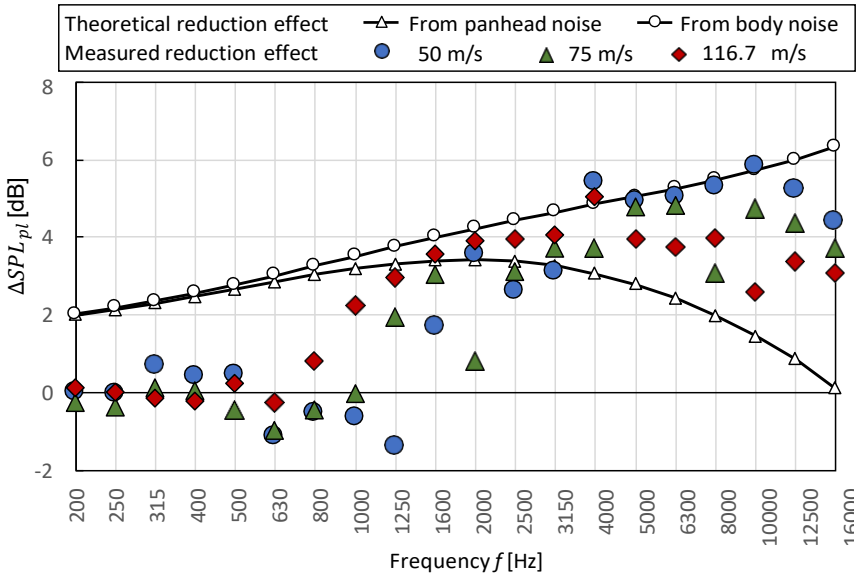


Fig. 14 Theoretical and measured noise levels reduced by sound insulating plate at 1/3 octave band frequency. Theoretical values from pantograph's panhead noise and from its body noise are plotted with white triangle dots and white circle dots. Measured values at 50, 75, and 116.7 m/s are plotted with blue circle dots, green triangle dots, and blue circle dots.

### 3.3.3 Estimation by similarity law

To evaluate the similarity law, the noise levels of the full-scale pantograph with and without the sound insulating plate at a wind velocity $U$ of 116.7 m/s were estimated from the measured noise levels of the 1/10 reduced-scale model at $U$ = 50 m/s and $U$ = 116.7 m/s. The value $SPL_{est,dD}$ was calculated by using Eqs. (2) and (16). Equation (16) is transformed from Eq. (1) for adopting the wind velocity and model scale conversion. $SPL_{est,}$ was calculated by using Eqs. (2) and (17) for adopting only the model scale conversion.

$$SPL_{est,VdD} = SPL_{mea,=50m/s} + 60\log\left(\frac{116.7m/s}{50m/s}\right) + 20\log 10 \quad (16)$$

$$SPL_{est,} = SPL_{mea,U=116.7m/s} + 20\log 10 \quad (17)$$

In addition, the noise level with the sound insulating plate was estimated by using the theoretical noise reduction effect of the sound insulating plate because the theoretical noise reduction can be adapted regardless of wind velocity. The value $SPL_{est,dD,red}$ was calculated by using Eqs. (2) and (18). In Eq. (18), the theoretical noise reduction of the sound insulating plate for the pantograph body, $\Delta SPL_{b,the}(f)$, is subtracted from the estimated noise level of the pantograph without the plate because the noise reduction for the pantograph body, $\Delta SPL_{b,the}(f)$, was closer to the measured value than that for the panhead in Fig. 14.

$$SPL_{est,VdD,red} = SPL_{mea,=50m/s,w/o\ plate} + 60\log\left(\frac{116.7m/s}{50m/s}\right) + 20\log 10 - \Delta SPL_{b,the}(f) \quad (18)$$

Figure 15 shows the estimated noise levels of the full-scale pantograph with and without the sound insulating plate at a wind velocity $U$ of 116.7 m/s. Figure 15(A) shows that the noise level without the plate estimated from the measured values at 50 m/s, $SPL_{est,VdD}$, had the same tendency as that from the values at 116.7 m/s, $SPL_{est,D}$. This lead to the overall noise levels of $SPL_{est,dD}$ having a 0.4-dB difference from $SPL_{est,D}$. This was because the dominant peak noise was estimated precisely by using the wind velocity conversion as the sixth power of the wind velocity as a dipole sound source.

However, Fig. 15(B), which shows the pantograph noise with the sound insulating plate, indicates that $SPL_{est,dD}$ at a low frequency region less than 400 Hz was higher than $SPL_{est,D}$. This lead to the overall noise level of $SPL_{est,dD}$ being 2.5 dB higher than that of $SPL_{est,D}$, showing that the noise reduction effect of the sound insulating plate was underestimated in the conversion of wind velocity. This was caused by the frequency characteristics of the sound insulating plate's noise reduction effect. In this study, the pantograph noise level in a low frequency range at 50 m/s was not affected by the noise reduction of the sound insulating plate in contrast to that at 116.7 m/s, shown in Fig. 14.

Therefore, $SPL_{est,dD}$, at a low frequency, was higher when not including the noise reduction effect of the plate. The values estimated by using the theoretical noise reduction effect, $SPL_{est,dD,red}$, had the same tendency as $SPL_{est,D}$. This lead to the overall noise levels of $SPL_{est,dD,red}$ having a 0.8-dB difference from $SPL_{est,D}$. This was because the dominant peak noise was estimated precisely by using the wind velocity conversion and the noise level was reduced by the sound insulating plates.

From this result, it was found that the sound insulating plate, of which the noise reduction effect has a frequency characteristic, made the actual noise level increase less than the noise level conversion of wind velocity. This caused the noise reduction effect of the sound insulating plate to be underestimated. To solve this problem, the plate's theoretical reduced noise level was subtracted from the estimated noise level of the pantograph itself. This lead to the pantograph noise with the plate being estimated within a 0.8-dB difference.

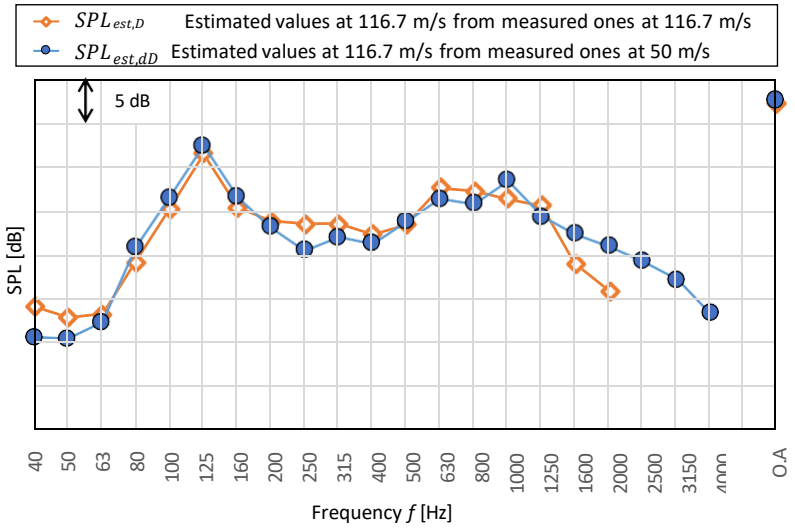


(a) Pantograph without sound insulating plate

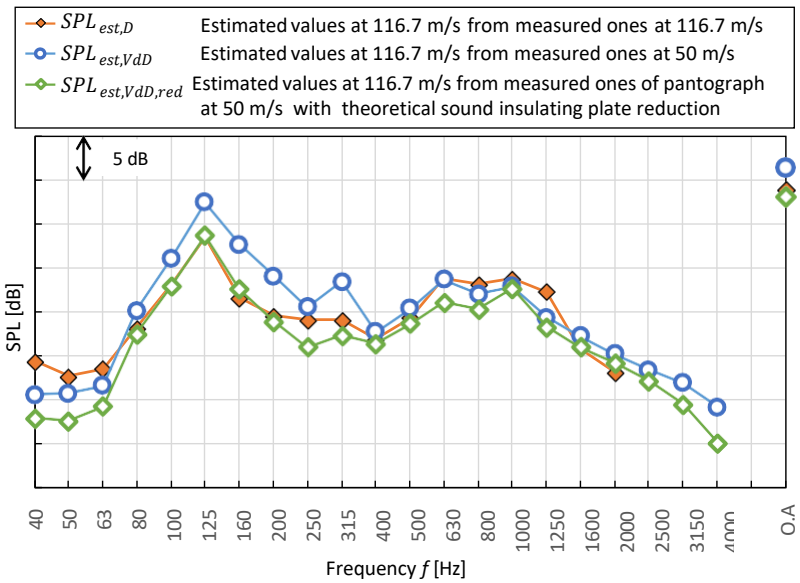


(b) Pantograph with sound insulating plate

Fig. 15 1/3 octave band frequency analysis of noise from measured and estimated values of 1/10-scale pantograph with and without sound insulating plate. Values estimated from measured values at 116.7 m/s by Eqs. (2) and (17) are plotted with orange and white rhombus dots. Values estimated from values at 50 m/s by Eqs. (2) and (16) are plotted with blue and white circle dots. Values estimated from values at 50 m/s by Eqs. (2) and (18) are plotted with green and white rhombus square dots.

## 4. Conclusion

In order to evaluate the sources of aerodynamic noise and the conversion of wind velocity according to the similarity law, we conducted measurements in a low-noise high-speed wind tunnel at flow rates greater than 100 m/s on cylinders with and without periodic holes, as well as on a pantograph model with and without a sound insulating plate. The wind tunnel's background noise increased as the wind speed increased from 60 m/s onwards, and then it increased as the wind speed increased from low to high speeds, eventually becoming proportional to the eighth power. The fact that this dependency exists demonstrates that the vortex's aerodynamic sound source, which originated in the shear layer near the nozzle, emerged as the primary quadrupole sound source.

In the Reynolds number range where the vortex formation remains constant, the cylinders' noise level increased as the sixth power of the wind velocity as a dipole sound source, according to measurements taken of both the with and without periodic holes cylinders. The noise reduction effect, caused by the change in flow structure, i.e., periodic holes, persisted independently of the wind velocity. Wind conversion using a dipole sound source overestimated the second peak noise emanating from the cylinders, which was proportional to the sixth and eighth powers of the wind velocity.

In comparison to the pantograph model operating as a dipole sound source, the noise level in the pantograph model with the sound insulating plate rose when the wind velocity decreased below the sixth power. Reason being, the sound insulating plate kept the rise in the low-frequency dominating noise level below the sixth power of the wind speed. When it came to lowering noise, the plate worked better at higher frequencies than lower ones. Furthermore, the pantograph noise's dominating frequency rose as the wind speed increased. Because of this, the significant noise level was impacted by the sound insulating plate's noise reduction. Because of the noise level conversion of wind velocity, the sound insulating plate's reduction impact was 2.5 dB understated. Subtracting the pantograph's estimated noise level from the theoretical lowered noise level of the plate, which was determined using the Fresnel number, allowed us to address this issue. This resulted in pantograph noise, with an estimated sound insulating plate differential of just 0.8 dB.

According to these findings, with wind velocities up to 116.7 m/s, the dipole sound-radiated noise level from the pantograph and cylinders rose continuously with the sixth power. The shorter turbulent correlation length causes a quadrupole sound source to rise, which in turn causes higher-frequency noise to grow in proportion to the sum of the sixth and eighth powers of the wind velocity. Furthermore, it was shown that items having a sound-insulating construction had a noise level below the sixth power of the wind speed. Finally, a noise level estimate based on wind velocity conversion might provide different results than the real noise level. The similarity rule should be used with caution when estimating the noise level of a full-scale train moving on a reduced-scale model with a variable wind velocity.

## References


Curle, N., The Influence of Solid Boundaries upon Aerodynamic Sound, Proceedings of the Royal Society of London, Series A, Mathematical and Physical Sciences, Vol. 231 (1955), pp. 505–514.

Fujita, H., Suzuki, H., Nagarekawa, H., Sagawa, A., and Takaishi, T., The Aeolian Tone Characteristics of a Circular Cylinder in High Reynolds Number Flow, 5th AIAA/CEAS Aeroacoustic Conference (1999), Paper No. AIAA- 99–1849.

Hitachi, Ltd., News release (2014) (in Japanese), http://www.hitachi.co.jp/New/cnews/month/2014/04/0407.html.

Howe, M., S., Theory of Vortex Sound, Cambridge University Press (2003) pp. 29-36.

Iida, A., Otaguro, T., Nagarekawa, H., Torii, A., and Naruse, I., Similarity Law of Aerodynamic Noise Generation, 6th AIAA/CEAS Aeroacoustic Conference (2000), Paper No. AIAA-2000–2012.

Iida, A., Similarity of Scale Model Experiments on Aeroacoustics, Journal of the Acoustical Society of Japan, Vol. 63, No. 9 (2007), pp. 549–554 (in Japanese).

Kambe, T., Aerodynamic sound, Journal of the Acoustical Society of Japan, Vol. 45, No.1 (1988), pp. 53-61 (in Japanese).

Kurita, T., Development of External-Noise Reduction Technologies for Shinkansen High-Speed Trains, Journal of Environment and Engineering, Vol. 6, No. 4 (2011), pp. 805–819.

Lighthill, M. J., On Sound Generated Aerodynamically, Proceedings of the Royal Society of London, Series A, Mathematical and Physical Science, Vol. 211 (1952), pp. 564–587.

Maekawa, Z., Experimental Study on Acoustical Designing of a Screen for Noise Reduction, Journal of the Acoustical Society of Japan, Vol. 18, No. 4 (1962), pp. 187-196 (in Japanese)

Martens, A., Wedemann, J., Meunier, N., and Leclere, A., High Speed Train Noise-Sound Source Localization at Fast Passing Trains, Deutsche Bahn AG, Sociedad Espanola de Acustica, S.E.A., (2009).

Matsui, A., Watanabe, T., and Abe, Y., Aerodynamic Force and Moment Measurement for Crosswind Stability Assessment in a Compact Wind Tunnel, Mechanical Engineering Journal, Vol. 4, No. 3, (2017), DOI: 10.1299/mej.17-00034

Takaishi, T., Ikeda, M., and Kato, C., Effects of Periodic Holes on the Suppression of Aeroacoustic Noise from a Pantograph Horn, Proceedings of ASME FEDSM'03 4th ASME/JSME Joint Fluids Engineering Conference (2003), Paper No. FEDSM2003-45464, p. 41-48.

Wakabayashi, Y., Kurita, T., and Horiuchi, M., Development of Pantograph Noise Insulating Panels, JR EAST Technical Review, No. 12 (2008), pp. 28–33.

Yamamoto, K. and Takagi, K., Expressions of Maekawa's Chart for Computation, Journal of the INCE of Japan, Vol. 15 No. 4 (1991), pp. 202–205 (in Japanese).

Yamamoto, K., Hotta, R., and Takagi, K., A Method for the Calculation of Noise Attenuation by Finite Length Barrier, Journal of the Acoustical Society of Japan, Vol. 50, No. 4 (1994), pp. 271–278 (in Japanese).

Yamazaki, N. and Takaishi, T., Wind Tunnel Tests on Reduction of Aeroacoustic Noise from Car Gaps and Bogie Sections, Quarterly Report of RTRI, Vol. 48, No. 4 (2007), pp. 229–235.